Characterizing mega-city pollution with TES O3 and CO measurements

C. Shim, Q. Li, M. Luo, S. Kulawik, H. Worden, J. Worden, A. Eldering, G. Diskin, G. Sachse, A. Weinheimer, et al.

Atmos. Chem. Phys. Discuss., 7, 15189–15212, 2007
www.atmos-chem-phys-discuss.net/7/15189/2007/

Atmospheric Chemistry and Physics Discussions

Characterizing mega-city pollution with TES O_3 and CO measurements

C. Shim[1], Q. Li[1], M. Luo[1], S. Kulawik[1], H. Worden[1], J. Worden[1], A. Eldering[1], G. Diskin[2], G. Sachse[2], A. Weinheimer[3], D. Knapp[3], D. Montzca[3], and T. Campos[3]

[1]Jet Propulsion Laboratory, California Institute of Technology, CA, USA
[2]NASA Langley Research Center, CO, USA
[3]National Center for Atmospheric Research (NCAR), VA, USA

Received: 28 August 2007 – Accepted: 11 September 2007 – Published: 25 October 2007

Correspondence to: C. Shim (cshim@jpl.nasa.gov)

Abstract

Concurrent tropospheric O_3 and CO vertical profiles from the Tropospheric Emission Spectrometer (TES) during the MILAGRO/INTEX-B aircraft campaigns over the Mexico City Metropolitan Area (MCMA) allow us to characterize mega-city pollution. Outflow from the MCMA occurred predominantly at 600–800 hPa, evident in O_3, CO, and NO_x enhancements in the in situ observations. We examined O_3, CO, and their correlation at 600–800 hPa from TES retrievals, aircraft measurements, and GEOS-Chem model results over the aircraft coverage (within a radius of ~700 km around MCMA). The enhancements in O_3 and CO seen in the in situ measurements are not apparent in TES data, due to the lack of TES coverage during several strong pollution events. However, TES O_3 and CO data are consistent with the aircraft observations on a daily mean basis (50–60 ppbv and 100–130 ppbv for O_3 and CO respectively). The O_3-CO correlation coefficients and enhancement ratios ($\Delta O_3/\Delta CO$) derived from TES data are in good agreements with those derived from the aircraft observations and GEOS-Chem model results (r:0.5–0.9;$\Delta O_3/\Delta CO$: 0.3–0.4), reflecting significant springtime photochemical production over MCMA and the surrounding region.

1 Introduction

Pollution in mega-cities (urban agglomerations with more than 10 million inhabitants) is a major environmental problem in the world (Fuchs et al., 1994) with consequences of air quality, climate change, and human health (Mage et al., 1996; Molina and Molina, 2004). The air quality in the Mexico City Metropolitan Area (MCMA: ~19° N, ~99° W, ~750 hPa) has become a top environmental concern. The MCMA has a population of over 18 million within an area of ~1500 km^2 located in a basin at an elevation of 2.2 km (~750 hPa). At such altitude the low partial pressure of oxygen leads to incomplete combustion hence large emissions of air pollutants from the MCMA. For example, in 1998, CO and VOCs emissions from the MCMA were ~1.8 Tg yr^{-1} and ~0.48 Tg C yr^{-1},

ACPD

7, 15189–15212, 2007

respectively (CAM, 2001). In addition, the surrounding mountains and boundary layer thermal inversions often trap pollution within the basin (Molina and Molina 2002).

CO is a good tracer for industrial and biomass burning pollution (Logan et al., 1981). The O_3-CO relationship, among other tracer-tracer correlations, has been used for ozone source attribution. For example, it has been well established that positive O_3-CO correlations provide a reliable characterization of continental pollution outflow (Fishman and Seiler, 1983; Chameides et al., 1987; Parrish et al., 1993). The O_3-CO correlation also provides a way to evaluate the photochemical O_3production in chemistry transport models (Chin et al., 1994).

The Tropospheric Emission Spectrometer (TES) aboard the Aura satellite provides concurrent mapping of global tropospheric O_3 and CO (Beer, 2006). Zhang et al. (2006) compared global TES O_3-CO correlations at 618 hPa with GEOS-Chem model results in an attempt to map the summertime continental pollution outflow. They showed that the TES data and GEOS-Chem results show consistent positive O_3-CO correlations and $\Delta O_3/\Delta CO$ over the continental outflow regions.

In the present study we examine TES O_3 and CO and their correlations over the MCMA and surrounding regions during the MILAGRO/ INTEX-B campaigns in March 2006 (Singh et al., 2006). The results are then compared with aircraft measurements from the same campaigns. We intend to identify characteristics of the MCMA pollution outflow on a regional to continental scale with TES data. Taking advantage of airborne measurements over MCMA, we first evaluate TES data to capture the regional pollution outflow with in situ measurements. The GEOS-Chem results are also compared with the aforementioned data. We describe the aircraft measurements, TES retrievals, and GEOS-Chem model in Sect. 2. Spatial distributions and temporal variations of O_3, CO and O_3-CO correlations from those data over MCMA and surrounding region are shown in Sect. 3. Conclusions are given in Sect. 4.

ACPD
7, 15189–15212, 2007

2 Methodology

2.1 Aircraft measurements

The MILAGRO (http://www.windows.ucar.edu/tour/link=/milagro/other_sites.html) and INTEX-B (Singh et al., 2006) aircraft campaigns in March 2006 focused on understanding the export and physiochemical evolution and removal of pollutants from the MCMA. A suite of chemical tracers including O_3, CO, NO_x, and VOCs (e.g., iso-pentane) were measured onboard the NSF C-130 and NASA DC-8 aircrafts over the MCMA. Figure 1 shows the flight tracks of C130 and DC8 during the campaigns. We focus our analysis on O_3 and CO measurements during 4 March–31 March 2006. The O_3 and CO data from C130 are measured by ChemiLuminescence Detector (CLD) and Tunable Diode Laser (TDL) respectively (Madronich et al., 2004). Those data from DC8 are measured by Langley in situ fast response ozone measurement (FASTOZ, Avery et al., 2001) and differential absorption CO measurement (DACOM, Novelli et al., 1994).

2.2 TES Data

The TES sensor onboard the Aura satellite provides global three-dimensional mapping of O_3 and CO among other trace gases (Beer, 2006). It measures infrared emissions with high spectral resolution (0.1 cm^{-1}) and a wide spectral range (measurements taken from 660–2260 cm^{-1}) (Beer et al., 2001). The ascending node of the Aura satellite passes the equator at 01:45 and 13:45 local time in a polar sun-synchronous orbit at 705 km altitude. In the nadir-viewing mode, TES has a nadir footprint of ~5×8 km, about 180 km apart between consecutive measurements along the orbital track and takes 16 days for global coverage (global survey). The TES special observation modes including the so-called "Step and Stare" with denser nadir spatial coverage, about 40 km apart along the orbit, and typically covers a 60° latitudinal range (Beer et al., 2006). We use here O_3 and CO data from 11 Step and Stares and five global surveys for March 2006 (Fig. 2).

ACPD
7, 15189–15212, 2007

TES optimal retrieval method for O_3 and CO profiles is based on Rodgers (2000). The retrieved profile (x_{ret}) may be expressed as the linear combination of the weighted true profile (x) and the a priori profile (x_a),

$$x_{ret} = Ax + (I - A)x_a + \mathbf{G}\varepsilon \quad (1)$$

where A is the averaging kernel (sensitivity of the retrieved profile to the perturbations of the true state), **G** is the gain matrix converting the noise to spectral measurement, and ε is the radiance measurement noise. The a priori profile (x_a) is constrained from monthly mean profiles of MOZART model (Brasseur et al., 1998). The details of the retrieval algorithms for O_3 and CO are described in Worden et al. (2004), Bowman et al. (2006), and Luo et al. (2007a) . Here we use the version 2 data (V002, F03_03) (Osterman et al. 2006). The degrees of freedom for signal (DOFS) for O_3 and CO in this study are about 1.6 and 1.2, respectively (Worden et al., 2004; Bowman et al., 2006).

The typical averaging kernels for O_3 and CO from TES Step & Stare observations over the MCMA are shown in Fig. 3. Both show significant sensitivities to 600–800 hPa, roughly the pressure level of the MCMA. Thus the TES data are sensitive to the pollution outflow over this region.

2.3 GEOS-Chem

GEOS-Chem is a global 3-D chemical transport model driven by assimilated meteorological data from NASA Global Modeling Assimilation Office (GMAO) (Bey et al., 2001). We use version 7-04-10 with a horizontal resolution of 2°×2.5° and 30 vertical layers of GEOS-4 (http://www.as.harvard.edu/chemistry/trop/geos). The 3-D meteorological fields are updated every six hours, and the surface fields and mixing depths are updated every three hours. GEOS-Chem includes a comprehensive tropospheric O_3-NO_x-VOC chemistry mechanism.

Climatological monthly mean biomass burning emissions are from Duncan et al. (2003). The fossil fuel emissions are from the Emission Database for Global At-

mospheric Research inventory (EDGAR) for NO_x, CO, and SO_2 and from the Global Emission Inventory Activity (GEIA) for other chemical compounds (Benkovitz et al., 1996; Olivier et al., 2001). These emissions are updated with particular national emission inventories and fuel use data: the Big Bend Regional Aerosol and Visibility Observational Study (BRAVO) inventory for Mexico (Kuhns et al., 2005) and U.S. EPA NEI 99 inventory (National Emissions Inventory, base year 1999, version 3) for the continental U.S. (EPA, 2004). The biogenic VOCs emissions are based on the Model of Emissions of Gases and Aerosols from Nature (MEGAN) inventory (Guenther et al., 2006). The lightning NO_x emissions use the parameterization based on the cloud top height and regionally scaled to the climatological Optical Transient Detector-Lightning Imaging Sensor (OTD-LIS) satellite observations of flash rates (Hudman et al., 2007). We conducted GEOS-Chem simulations for September 2005–March 2006 with the first six months for initialization. We focus our analysis on March 2006. For direct comparison, model results are sampled along the aircraft flight tracks as well as TES orbital tracks.

In order to compare GEOS-Chem with the TES retrievals, the model profiles of O_3 and CO are convoluted with TES averaging kernels to account for the different sensitivities and a priori information of TES retrievals to different pressure levels (Jones et al., 2003; Richards et al., 2007[1]). The resulting transformed model profile can then be directly compared with TES retrievals without bias associated with the TES ta priori information and vertical resolution (Zhang et al., 2006; Jourdain et al., 2007; Worden et al., 2007). TES averaging kernels were not applied to the aircraft profiles due to the scarcity of temporal and spatial coincidence between TES and aircraft measurements (Luo et al., 2007b).

[1] Richards, N. A. D., Osterman, G. B., Browell, E. V., et al.: Validation of Tropospheric Emission Spectrometer (TES) Ozone Profiles with Aircraft Observations During INTEX-B, J. Geophys. Res., in review, 2007.

3 Results and discussions

3.1 Mexico City pollution outflow

The vertical profiles of O_3, CO, and NO_x mixing ratios from the aircraft measurements during MILAGRO/INTEX-B are shown in Fig. 4. There are generally higher concentrations in the C130 measurements than those in the DC8 data. This is due largely to the closer proximity of the C130 flights to the MCMA (Fig. 1). Pollution outflow from the MCMA occurs mainly at 600–800 hPa, as indicated by the enhanced O_3, CO, and NO_x levels, reflecting the high elevation of the region (~750 hPa). Since TES retrieval over this region has maximum sensitivity around 600–800 hPa (see Sect. 2.2), TES tropospheric O_3 and CO profiles thus provide unique insight into the emissions, chemistry, and transport around the MCMA.

4 Spatial distributions of tropospheric O_3 and CO over the MCMA

Figure 5 shows the mean O_3 concentrations at three pressure bins (>800 hPa, 600–800 hPa, and 400–600 hPa) during the MILAGRO/INTEX-B campaigns. We do not include the upper troposphere (<400 hPa) in our analysis since there were no measurements by C130 above ~350 hPa. The aircraft data are averaged onto $1^\circ \times 1^\circ$ grids to account for finer temporal and spatial scales of aircraft observations (left panel, Fig. 5). TES retrievals are selected when aircraft measurements are available on a daily basis and are then averaged onto $2^\circ \times 2.5^\circ$ grids to compare with GEOS-Chem results (middle panel, Fig. 5). The GEOS-Chem model results are sampled along TES orbital tracks with TES averaging kernels applied (right panel, Fig. 5). Typical error due to the spatial and temporal difference between TES and GEOS-Chem model profiles is about 5% (Zhang et al., 2006). The O_3 concentrations from the aircraft measurements, TES retrievals, and GEOS-Chem results are fairly comparable at >800 and 400–600 hPa (40–50 ppbv). However, the significant O_3 enhancement (>60 ppbv) seen

ACPD
7, 15189–15212, 2007

EGU

in the aircraft data at 600–800 hPa is not apparent in either TES or GEOS-Chem profiles (middle left panel, Fig. 5). As explained in Sect. 2.3, TES averaging kernels were not applied to aircraft measurements for the comparison; that sharp enhancement of aircraft O_3 could be smeared or reduced if the TES averaging kernel were applied to aircraft measurements. We will further discuss this discrepancy in Sect. 3.3.

Figure 6 shows the mean CO mixing ratios at three pressure bins (>800 hPa, 600–800 hPa, and 400–600 hPa) during the MILAGRO/INTEX-B campaigns. TES CO concentrations show no bias compared with aircraft measurements at 400–600 hPa. However, the large CO enhancements (>120 ppbv) at surface – 600 hPa seen in the in situ measurements are not apparent in the TES data. GEOS-Chem results, when convoluted with TES averaging kernels underestimate the aircraft measurements by 10–31 ppbv. We will also further discuss this discrepancy in Sect. 3.3.

4.1 Daily variabilities of O_3 and CO over the MCMA

The time series of daily mean O_3 and CO of aircraft measurements, TES retrievals and GEOS-Chem results at 600–800 hPa over the aircraft coverage (within a radius of ~700 km, middle left panel, Fig. 5) are shown in Fig. 7. These comparisons are of particular importance since most of the emissions of air pollutants are from the high-elevation Mexico City basin, and the discrepancies of monthly averages between the three data sets are largest. Clearly there are five high-pollution days: 67th, 69th, 75th, 81st, and 88th Julian day when daily mean O_3 and CO concentrations are higher than 60 ppbv and 150 ppbv, respectively. Figure 7 shows daily mean TES retrievals over the regions covered by all the aircraft measurements during the aircraft campaigns (middle left panel, Fig. 5, green diamonds with standard deviation) and shows daily mean TES retrievals only co-located with the daily aircraft coverage (red crosses). The red crosses represent more direct comparison with aircraft measurements. As shown in Fig. 7, TES coverage is limited missing the three severe pollution days (67th, 81st, and 88th), which leads to negative bias of monthly mean TES O_3 and CO during this campaign.(−4.4 ppbv (Fig. 5) and −20 ppbv (Fig. 6) respectively). However, the

ACPD
7, 15189–15212, 2007

TES mean values on the days of coincident measurement with aircraft data are in better agreement (+0.3 ppbv for O_3 and −14 ppbv for CO). Considering the standard deviations of daily mean TES CO (±17 ppbv) and that of daily aircraft CO (>±20 ppbv), TES CO is still comparable with aircraft measurements. Daily GEOS-Chem O_3 and CO without applying TES averaging kernel are significantly underestimated by ∼29% (−13 ppbv) and ∼45% (−51 ppbv), respectively and the simulated temporal variation is not consistent with TES.

4.2 The O_3–CO relationship over the MCMA

We estimate the O_3-CO correlations derived from aircraft measurements, TES retrievals, and GEOS-Chem with TES averaging kernels applied during the MILAGRO/INTEX-B experiments. All the data for O_3-CO correlations are gridded onto 2°×2.5° grids for consistency with GEOS-Chem results. The correlations are estimated over the flights coverage (14° N–35° N and 90° W–103° W, colored area at left panels, Fig. 5). We computed O_3-CO linear regressions using the reduced major axis method taking account of both variables' error estimates (Hirsh and Gilroy, 1984). The resulting slope represents $\Delta O_3/\Delta CO$ enhancement ratio. Figure 8 shows the O_3-CO correlation at the three pressure bins (>800 hPa, 600–800 hPa, and 400–600 hPa) and those results are compared with other observations in Table 1.

Below 800 hPa, the correlation coefficient (R=0.47) and $\Delta O_3/\Delta CO$ enhancement ratio (0.38±0.13 mol mol^{-1}) derived from TES tropospheric retrievals are in close agreement with those for aircraft measurements (R=0.53 and $\Delta O_3/\Delta CO$=0.36 ±0.09 mol mol^{-1}). GEOS-Chem results show similar $\Delta O_3/\Delta CO$ enhancement ratio of 0.3±0.05 mol mol^{-1}, but with higher correlation coefficient (R=0.72). The lower correlation coefficient of TES data than that of model can be partly attributed to the spectral measurement error in TES retrievals, which reduces the O_3-CO correlation in TES data (Zhang et al., 2006).

At 600–800 hPa, TES results show lower correlation coefficient (R=0.50) and higher

ACPD
7, 15189–15212, 2007

$\Delta O_3/\Delta CO$ enhancement ratio (0.43 ± 0.09 mol mol^{-1}) than those of aircraft measurements (R=0.78 and $\Delta O_3/\Delta CO = 0.28\pm0.07$ mol mol^{-1}). The higher TES $\Delta O_3/\Delta CO$ enhancement ratio is due in part to the relatively negative bias in TES CO retrievals as explained in Sect. 3.3 However, TES results are roughly in good agreement with the aircraft measurement. Those values are close to those derived from summertime in situ measurements over the Eastern U.S. at surface and lower troposphere: R=0.7–0.9 and $\Delta O_3/\Delta CO$=0.2–0.4 mol mol^{-1} (Parrish et al., 1993; Chin et al., 1994); and those from the Intercontinental Chemical Transport Experiment – North America (INTEX-NA) experiments (July–August 2004, surface – 600 hPa): R=0.5–0.67 and $\Delta O_3/\Delta CO$=0.31–0.44 mol mol^{-1}. GEOS-Chem results shows closer values to those of aircraft measurements (R=0.58 and $\Delta O_3/\Delta CO=0.25\pm0.06$ mol mol^{-1}) as well. These similarities imply that substantial springtime pollutions and photochemical production over the elevated MCMA (600–800 hPa) and surrounding regions (middle left, Fig. 5) in the lower latitude (14° N–35° N). The correlation of GEOS-Chem results without TES averaging kernel is shown in Table 1 to see the influence of TES averaging kernel on the correlation. The $\Delta O_3/\Delta CO$ enhancement ratio is comparable ($\Delta O_3/\Delta CO=0.3\pm0.15$ mol mol^{-1}) to reflect photochemical O_3 productions in the model. However, there is much weaker correlation (R=0.26), which imply the emission inventories of O_3 precursors over MCMA are largely underestimated in the model (Fig. 7). The $\Delta O_3/\Delta CO$ enhancement ratio for the Transport and Chemical Evolution over the Pacific (TRACE-P, March–April 2001) aircraft mission is smaller ($\Delta O_3/\Delta CO$=~0.15, surface – 600 hPa) than that of MILAGRO/INTEX-B, likely due to less active photochemistry over springtime middle latitudes over the western Pacific (Jacob et al., 2003).

At 400–600 hPa in the middle to upper troposphere, both TES and aircraft data show relatively high CO-O_3 correlation coefficient (R=0.59 and 0.86, respectively) and $\Delta O_3/\Delta CO$ enhancement ratio (0.37 ± 0.08 mol mol^{-1} and 0.44 ± 0.04 mol mol^{-1}, respectively). The higher enhancement ratio and correlation coefficient are likely due to a larger dynamic range of O_3 in the middle to upper troposphere. However, these enhancement ratios are smaller than that of in situ measurements from TES results

(July 2005, 618 hPa, $\Delta O_3/\Delta CO$=0.81 mol mol^{-1}) and the ICARTT aircraft campaign (July–August 2004, 600–650 hPa, $\Delta O_3/\Delta CO$=0.72 mol mol^{-1}) reported by Zhang et al. (2006). The higher slopes possibly reflect different photochemical and dynamic environments of free troposphere in different seasons.

5 Conclusions

We examined O_3, CO, and their relationships from TES tropospheric retrievals, aircrafts observations, and GEOS-Chem model results over the MCMA and surrounding region (14N°–35° N and 90° W–103° W) during MILAGRO/INTEX-B (March 2006). The typical TES averaging kernels of O_3 and CO over the MCMA have high sensitivity at 600–800 hPa. Given the high altitude of the MCMA (~750 hPa), TES data are thus suitable for analyzing the pollution outflow from this region.

We first evaluated TES tropospheric O_3 and CO mixing ratio profiles and their correlations against those from the in situ aircraft measurements. Several of the main pollution outflow events observed by aircrafts did not have collocated TES overpasses. There are good agreements between collocated TES and aircraft measurements of O_3 and CO mixing ratios on a daily mean basis during MILAGRO/INTEX-B. GEOS-Chem results of O_3 and CO mixing ratios are significantly lower than the in situ values.

The correlation coefficients and $\Delta O_3/\Delta CO$ enhancement ratios from the three data sets (TES, in situ, GEOS-Chem) show comparable values (r=0.5–0.9; $\Delta O_3/\Delta CO$=0.3–0.4) at three pressure bins (>800 hPa, 800–600 hPa, and 400–600 hPa). TES correlation coefficients for all three pressure bins are in the range of 0.47–0.59. The $\Delta O_3/\Delta CO$ enhancement ratio of 0.3–0.4 mol mol^{-1} from this study is consistent with that of summertime values at surface over the eastern US (Parrish et al., 1993; Chin et al., 1994). The O_3-CO relationships during MILAGRO/INTEX-B therefore imply vigorous springtime photochemical O_3 production over the MCMA and surrounding region. The results presented here suggest that TES tropospheric O_3 and CO profile retrievals can be used

ACPD
7, 15189–15212, 2007

to characterize mega-city pollution outflow on a regional to global scale.

Acknowledgements. This work is performed at the Jet Propulsion Laboratory (JPL), California Institute of Technology, under contract with the NASA. C. Shim and Q. Li were jointly supported by the JPL Research and Technology Development program, Human Resources Development Fund, NASA Atmospheric Composition Modeling and Analysis program, and the TES project at JPL. The GEOS-Chem model is managed at Harvard University with support from the NASA Atmospheric Chemistry Modeling and Analysis Program. We thank M. Avery for the in-situ O_3 measurements. We are also grateful to S. Madronich, L. Molina, J. Gaffney, and H. Singh for organizing the aircraft campaign.

References

Avery, M. A., Westberg, D. J., Fuelberg, H. E., et al.: Chemical transport across the ITCZ in the central Pacific during an El Niño-Southern Oscillation cold phase event in March–April 1999, J. Geophys. Res., 106 (D23), 32 539–32 554, doi:10.1029/2001JD000728, 2001.

Beer, R. and TES on the Aura Mission: Scientific objectives, measurements and analysis overview, IEEE Trans. Geosci. Remote. Sens., 44, 1102–1105, 2006.

Beer, R., Glbavich, T. A., and Rider, D. M.: Tropospheric emission spectirometer for the Earth Observing System's Aura satellite, Appl. Opt. 40, 2356–2367, 2001.

Benkovitz, C. M., Scholtz, M. T., Pacyna, J., et al.: Global gridded inventories of anthropogenic emissions for sulfur and nitrogen, J. Geophys. Res., 101 (D22), 29 239–29 253, 1996.

Bey, I. Jacob, D. J., Yantosca, R. M., et al.: Global modeling of tropospheric chemistry with assimilated meteorology: Model description and evaluation, J. Geophys. Res., 106(D19), 23 073–23 096, 2001.

Bowman, K. W., Rodgers, C. D., Kulawik, S. S., et al.: Tropospheric emission spectrometer: Retrieval method and error analysis, IEEE Trans. Geosci. Remote. Sens., 44, 1297–1307, 2006.

Braseur, G. P. Hauglustaine, D. A., Walters, S., et al.: MOZART: A global chemical transport model for ozone and related chemical tracers, Part I: Model description, J. Geophys. Res., 103, 28 256–28 289, 1998.

CAM: Preliminary Emissions Inventory; INE, 2000b, Almanaque de Datos y Tendencias de la Calidad del Aire en Ciudades Mexicanas, 1998, 2001.

Chameides, W. L. David, D. D., Rodgers, M. O., et al.: Net ozone photochemical production over the eastern and central north Pacific as inferred from CTE/CITE 1 observations during fall 1983, J. Geosphys. Res., 92, 2131–2152, 1987.
Chin, M., Jacob, D. J., Munger, J. W., et al.: Relationship of ozone and carbon monoxide over North America, J. Geophys. Res., 99, 14 565–14 573, 1994.
Duncan, B. N., Martin, R. V., Staudt, A. C., et al.: Interannual and seasonal variability of biomass burning emissions constrained by satellite observations, J. Geophys. Res., 108(D2), 4100, doi:10.1029/2002JD002378, 2003.
EPA, U. S.: EPA Clearinghouse for inventories and emissions factors: 1999, National Emission Inventory Documentation and Data – Final Version 3.0, http://www.epa.gov/ttn/chief/net/1999inventory.html, 2004.
Fishman, J. and Seiler, W.: Correlative nature of ozone and carbon monoxide in the troposphere: Implications for the tropospheric ozone budget, J. Geosphys. Res., 88, 3662–3670, 1983.
Fuchs, R. J., Brennan, E., Chamie, J., et al.: Mega-city growth and the future, United Nations university press, Tokyo, 1994.
Guenther, A. B., Karl, T., Harley, P., et al.: Estimates of global terrestrial isoprene emissions using MEGAN (Model of Emissions of Gases and Aerosols from Nature), Atmos. Chem. Phys., 6, 3181–3210, 2006, http://www.atmos-chem-phys.net/6/3181/2006/.
Heald, C. L., Jacob, D. J., Jones, D. B. A, et al.: Comparative inverse analysis of satellite (MOPITT) and aircraft (TRACE-P) observations to estimate Asian sources of carbon monoxide, J. Geophys. Res., 109, D23306, doi:10.1029/2004JD005185, 2004.
Hirsch, R. M. and Gilroy, E. J.: Methods of fitting a straight line to data: Examples in water resources, Water Resour. Bull., 20 705–20 711, 1984.
Hudman, R. C., Jacob, D. J., Turquety, S., et al.: Surface and lightning sources of nitrogen oxides over the United States: Magnitudes, chemical evolution, and outflow, J. Geophys. Res., 112, D12S05, doi:10.1029/2006JD007912, 2007.
Jacob, D. J., Crawford, J. H., Kleb, M. M., et al.: Transport and Chemical Evolution over the Pacific (TRACE-P) aircraft mission : Design, execution, and first results, J. Geophys. Res., 108(D20), 9000, doi:10.1029/2002JD003276, 2003.
Jones, D. B. A., Bowman, K. W., Palmer, P. I., et al.: Potential of observations from the Tropospheric Emission Spectrometer to continental sources of carbon monoxide, J. Geophys.

Res., 108(D24), 4789, doi: 10.1029/2003JD003702, 2003.
Jourdain, L. and Hauglustaine, D. A.: The global distribution of lightning NOx simulated on-line in a general circulation model, Phys. Chem. Earth, C26, 585–591, 2001.
Jourdain, L., Worden, H. M., Worden, J. R., et al.: Tropospheric vertical distribution of tropical Atlantic ozone observed by TES during the northern African biomass burning season, Geophys. Res. Lett., 34, L04810, doi:10.1029/2006GL028284, 2007.
Kuhns, H., Knipping, E. M., Vukovich J. M., et al.: Development of a United States-Mexico Emissions Inventory for the Big Bend Regional Aerosol and Visibility Observational (BRAVO) Study, J. Air. Waste Manag. Assoc., 55(5), 677–92, 2005.
Luo, M., Rinsland, C., Fisher, B., et al.: Comparison of carbon monoxide measurements by TES and MOPITT: the influence of a priori data and instrument characteristics on nadir atmospheric species retrievals, J. Geophys. Res., 112, D09303, doi:10.1029/2006JD007663, 2007a.
Luo, M., Rinsland, C., Fisher, B., et al.: TES carbon monoxide validation with DACOM aircraft measurements during INTEX-B 2006, J. Geophys. Res., in press, 2007b.
Logan, J. A., Prather, M. J., Wofsy, S. C., et al.: Tropospheric Chemistry : A global perspective, J. Geophys. Res., 86, 7210–7254, 1981.
Madronich, S., Flocke, F., Orlando, J., et al.: MIRAGE-Mex: Mexico City Pollution Outflow Experiment: Science Overview Document, http://mirage-mex.acd.ucar.edu/Documents/MIRAGE-Mex_SOD_040324.pdf, 2004.
Mage, D., Ozolins, G., Peterson, P., et al.: Urban air pollution in megacities of the world, Atmos. Environ, 30(5), 681–686, 1996.
Molina, L. T. and Molina, M. J.: Air Quality in the Mexico Megacity, Kluwer Academic Publishers, Norwell, M.A., 2002.
Molina, M. J. and Molina, L. T.: Critical Review: Megacities and Atmospheric Pollution, J. Air & Waste Manage. Assoc., 54, 6, 644–680, 2004.
Novelli, P. C., Steele, L. P., Tans, P. P., et al.: Reevaluation of the NOAA /CMDL carbon monoxide reference scale and comparisons with CO reference gases at NASA-Langley and the Fraunhofer Institut, J. Geophys. Res., 99(D6), 12 833–12 840, 1994.
Olivier, J. G. J. and Berdowski, J. J. M.: Global emissions sources and sinks, in: "The Climate System", edited by: J. Berdowski, R. Guicherit, and B. J. Heij , pp. 33–78, A. A. Balkema Publishers/Swets & Zeitlinger Publishers, Lisse, The Netherlands, ISBN 90 5809 255 0., 2001.

Osterman, G., Bowman, K., Cady-Pereira, K., et al.: Tropospheric emission spectrometer (TES) validation report, JPL D33192, version 2.0 (available at http://eosweb.larc.nasa.gov/PRODOCS/tes/validation/TESValidationReport_v2_0.pdf), 2007.

Park, R. J., Jacob, D. J., Field, B. D., et al.: Natural and transboundary pollution influences on sulfate-nitrate-ammonium aerosols in the United States: Implications for policy, J. Geophys. Res., 109, D15204, doi:10.1029/2003JD004473, 2004.

Parrish, D. D., Holloway, J. S., Trainer, M., et al.: Export of North American ozone pollution to the North Atlantic Ocean, Science, 259, 1436–1439, 1993.

Rogers, C. D.: Inverse Methods for Atmospheric Sounding: Theory and Practice, World Sci., River Edge, N. J., 2000.

Singh, H. B., Brune, W. H., Crawford, J. H., et al.: The Intercontinental Chemical Transport Experiment – Phase B (INTEX-B): White Paper, (http://cloud1.arc.nasa.gov/docs/intex-na/INTEX-B_White_Paper.pdf), 2006.

Worden, H., Logan, J. A., Worden, J. R., et al.: Comparisons of Tropospheric Emission Spectrometer (TES) ozone profiles to ozonesodes: methods and initial results, J. Geophys. Res., 112, D03309, doi:10.1029/2006JD007258, 2007.

Worden, J., Kulawik, S. S., Shephard, M. W., et al.: Predicted errors of tropospheric emission spectrometer nadir retrievals from spectral window selection, J. Geophys., Res., 109, No. D9, D09308, 10.1029/2004JD004522, 2004.

Zhang, L., Jacob, D. J., Bowman, K. W., et al.: Ozone-CO correlations determined by the TES satellite instrument in continental outflow regions, Geophys. Res. Lett., 33, L18804, doi:10.1029/2006GL026399, 2006.

Table 1. O_3–CO correlation coefficients and slopes ($\Delta O_3/\Delta CO$).

Location		Time period	Pressure	r	$\Delta O_3/\Delta CO$	
MCMA	in situ	March 2006	600–800 hPa	0.78	0.28±0.07	
	TES			0.5	0.43±0.09	
	GC/AK[a]			0.58	0.25±0.06	
	GC-raw[b]			0.26	0.3±0.15	
Eastern U.S. (TES[c])		July 2005	618 hPa	0.53	0.81	Zhang et al. (2006)
Eastern U.S.		July–September, 2004	600 hPa–surface	0.5–0.7	0.31–0.44	ICARTT
Western Pacific		Feburary–March, 2001	600 hPa–surface	0.6	0.15	TRACE-P
Eastern U.S.		June–August, 1988–1991	surface	0.7–0.9	0.2–0.4	Chin et al. (1994)
Sable Island		July–September, 1991	surface	0.82	~0.3	Parrish et al. (1993)

[a]GEOS-Chem results with TES averaging kernels applied.
[b]GEOS-Chem results without applying TES averaging kernels. All MCMA data were averaged onto 2°×2.5° grids over the aircraft coverage (colored area, left panels in Fig. 5).
[c]TES version 1(V001) data averaged onto 10°×10° grid.

ACPD
7, 15189–15212, 2007

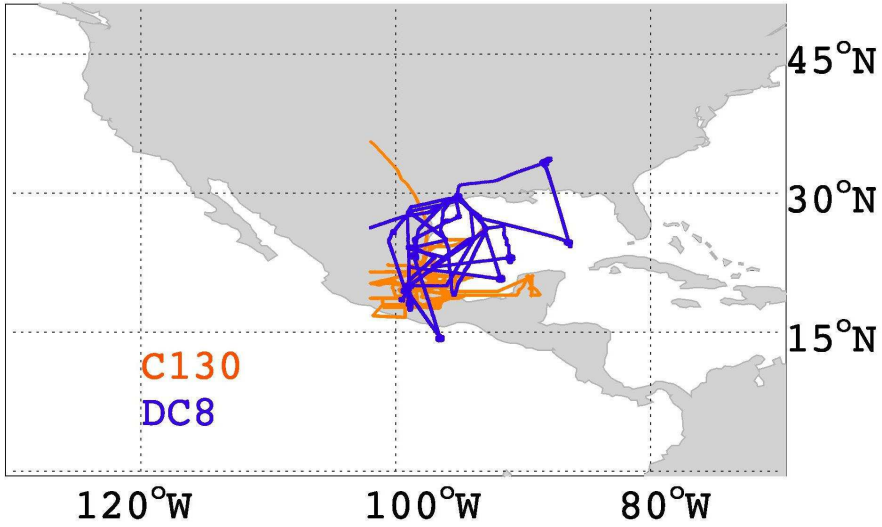

Fig. 1. The flight tracks of the C130 (orange) and DC8 (blue) aircrafts during the MILAGRO/INTEX-B (phase I) campaigns in March 2006.

ACPD
7, 15189–15212, 2007

EGU

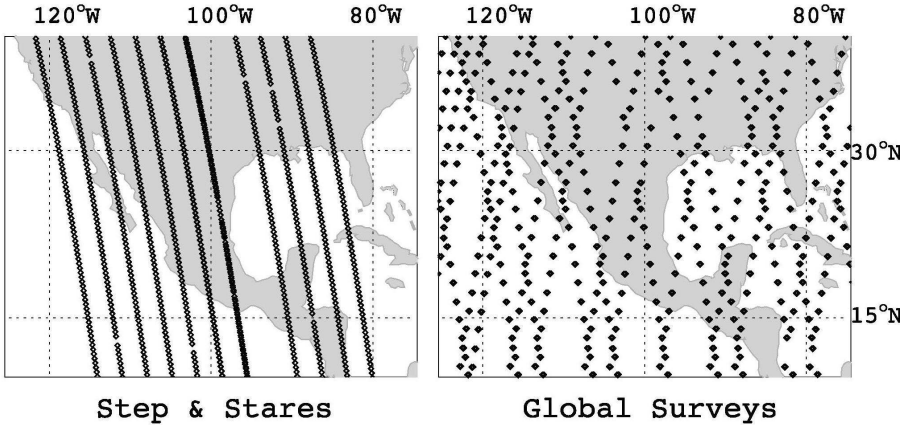

Fig. 2. Orbital tracks of 11 TES Step and Stares (left panel) and five Global Surveys (right panel) over the MILAGRO/INTEX-B (Phase I) region in March 2006.

ACPD
7, 15189–15212, 2007

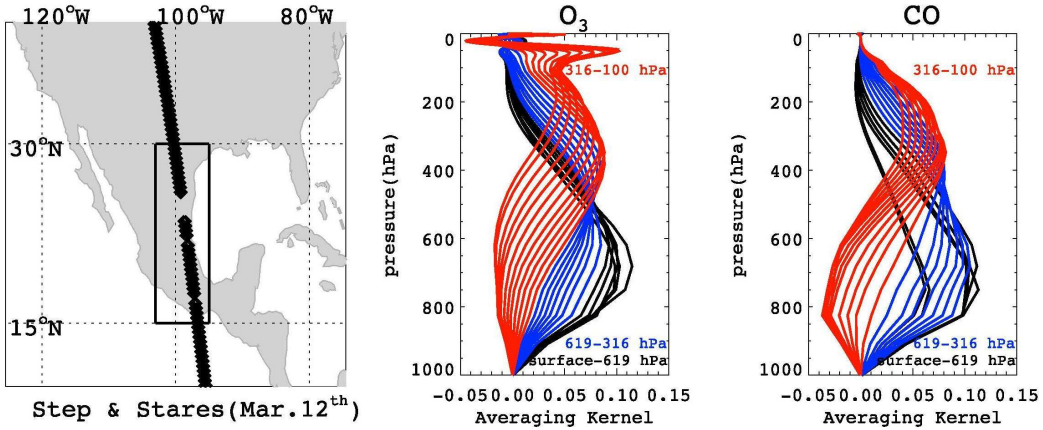

Fig. 3. Typical averaging kernels of O_3 (middle panel) and CO (right panel) for TES Step and Stares between 15–30° N (left panel) on 12 March 2006. Averaging kernels for different pressure levels are shown (color-coded).

ACPD
7, 15189–15212, 2007

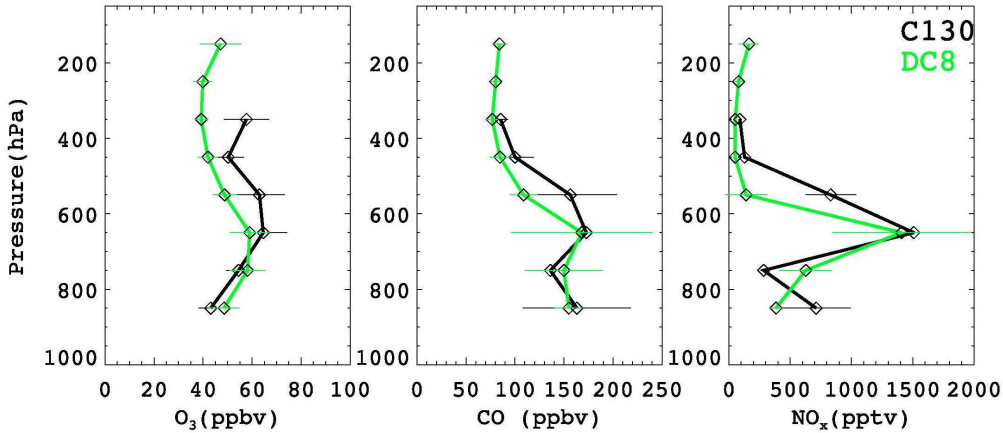

Fig. 4. The mean vertical profiles of O_3 (left panel), CO (middle panel), and NO_x (right panel) from the C130 (black) and DC8 (green) during MILAGRO/INTEX-B (Phase I). Standard deviations are shown for each pressure level.

ACPD
7, 15189–15212, 2007

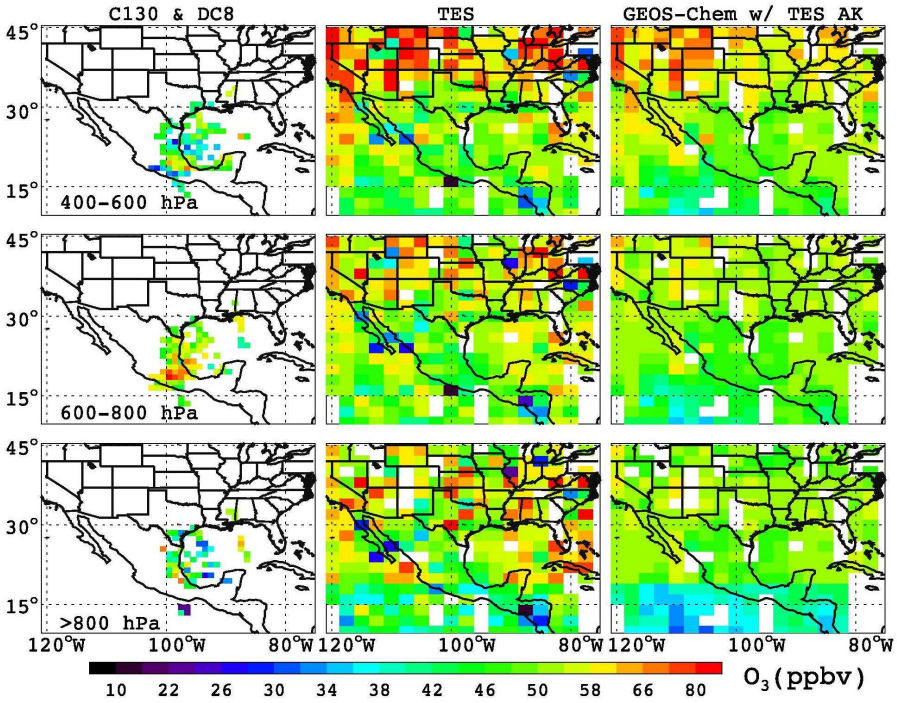

Fig. 5. Mean O_3 mixing ratios at 400–600 hPa, 600–800 hPa, and below 800 hPa during MILAGRO/INTEX-B (Phase I). The aircraft measurements are averaged onto 1°×1° grids (left panel). TES data are sampled on the days with aircraft flights and averaged onto 2°×2.5° grids (middle panel). GEOS-Chem results are sampled along the TES orbital tracks with TES averaging kernels applied (right panel).

ACPD
7, 15189–15212, 2007

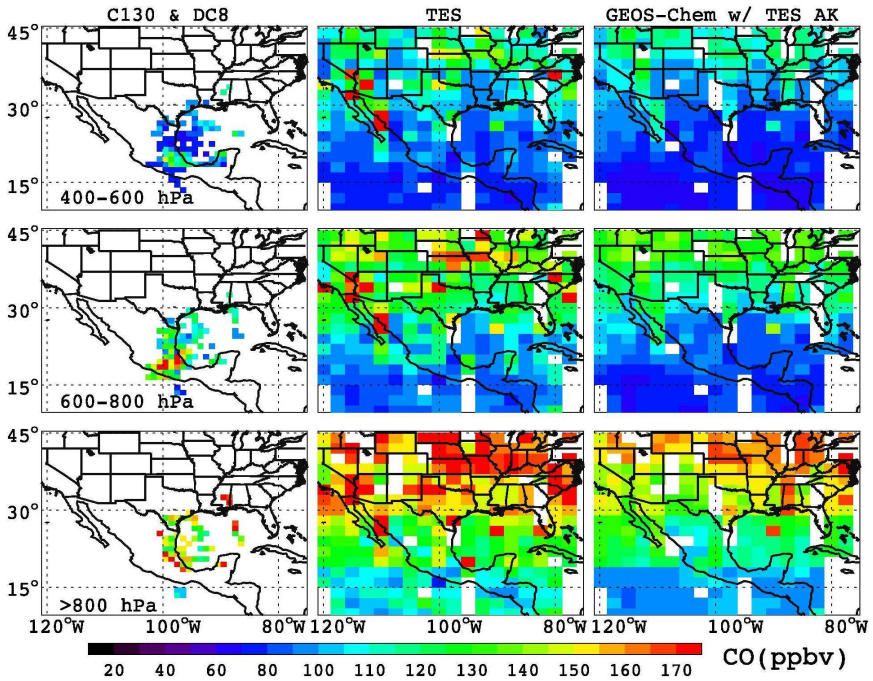

Fig. 6. Same as Fig. 5, but for CO.

ACPD
7, 15189–15212, 2007

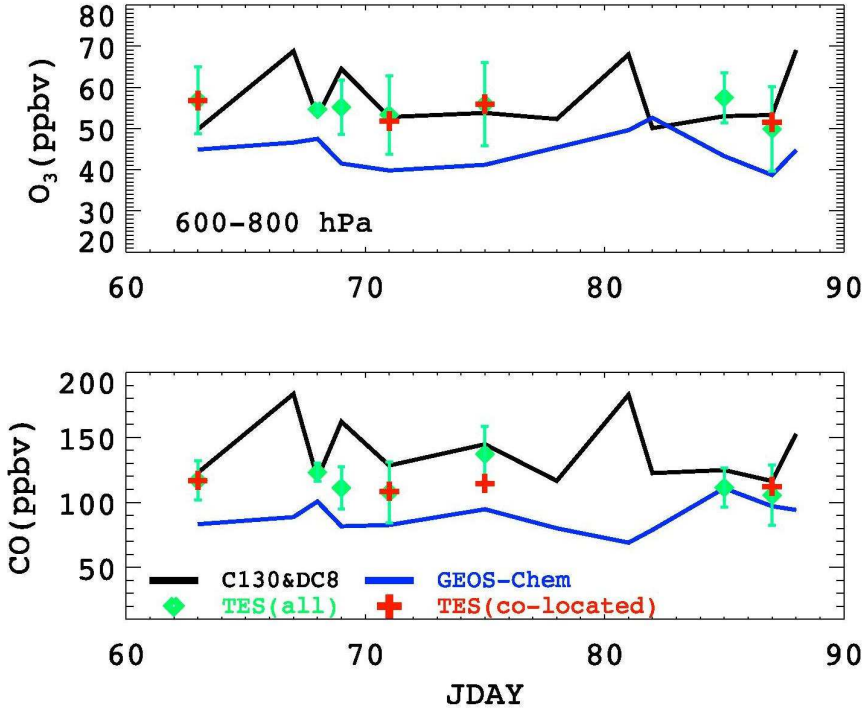

Fig. 7. Time series of daily mean O_3 (upper panel) and CO (lower panel) at 600–800 hPa during MILAGRO/INTEX-B (Phase I). Black solid lines – aircraft measurements; blue solid lines – GEOS-Chem results without applying TES averaging kernels; green diamonds – mean TES retrievals over the aircraft coverage at 600–800 hPa; red crosses – mean TES retrievals that have colocated aircraft measurements.

ACPD
7, 15189–15212, 2007

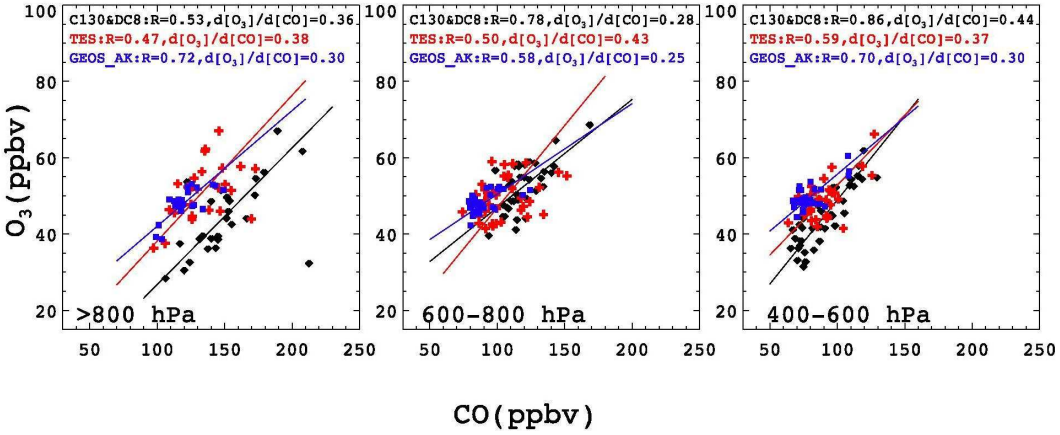

Fig. 8. CO-O_3 relationships at three pressure bins, below 800 hPa, 600–800 hPa, and 400–600 hPa during MILAGRO/INTEX-B (Phase I). Data were averaged onto 2°×2.5° grids over the aircraft coverage. Black diamonds – aircraft measurements; red crosses – TES retrievals on the days of the aircraft measurements; blue rectangles – GEOS-Chem results sampled along the TES orbital tracks with TES averaging kernels applied.

ACPD
7, 15189–15212, 2007